nature astronomy

LETTERS

https://doi.org/10.1038/s41550-020-1144-x

Check for updates

New maser species tracing spiral-arm accretion flows in a high-mass young stellar object

Xi Chen[1,2,3] ✉, Andrej M. Sobolev[4] ✉, Zhi-Yuan Ren[5], Sergey Parfenov[4], Shari L. Breen[6], Simon P. Ellingsen[7], Zhi-Qiang Shen[2,3], Bin Li[2,3], Gordon C. MacLeod[8,9], Willem Baan[10], Crystal Brogan[11], Tomoya Hirota[12,13], Todd R. Hunter[11], Hendrik Linz[14], Karl Menten[15], Koichiro Sugiyama[13,16], Bringfried Stecklum[17], Yan Gong[15] and Xingwu Zheng[18]

Numerical simulations have predicted that substructures such as spiral arms can be produced through a gravitationally unstable disk around high-mass young stellar objects (HMYSOs)[1–5]. Recent high-resolution observations from the Atacama Large Millimeter/submillimeter Array have investigated these substructures at a spatial resolution of ~100 au (refs. [6–10]). An accretion burst, which is a manifestation of an increase in the accretion rate caused by a gravitational instability in the disk[1,11,12], can result in luminosity outbursting phenomena—as has been seen in several HMYSOs[13,14]. However, no clear relationship between the accretion bursts and disk substructures has been established. Here we report the detections of three new molecular maser species, HDO, HNCO and $^{13}CH_3OH$, from the direction of the HMYSO G358.93-0.03 during a 6.7 GHz methanol maser flaring event[15]. High-quality imaging of the three new maser species exhibits consistent observational evidence that these masers closely trace the spiral-arm substructures around this HMYSO. The rapid decay of the spectral lines emitted from these molecules suggests that these are transient phenomena (for only ~1 month), probably associated with rapid changes in radiation field due to an accretion burst. Therefore, these new maser species provide evidence linking the spiral-arm substructure with an accretion burst, both expected from massive disk instabilities.

The methanol maser in the 6.7 GHz 5_0–6_1 (J_K–$J'_{K'}$) A^+ transition from the direction of G358.93-0.03 has been undergoing a period of flaring since January 2019 (ref. [15]). During this period, the 6.7 GHz maser emission has increased by two orders of magnitude from <10 Jy in early observations[15,16] to ~1,000 Jy in mid-March 2019[17,18]. Intensive monitoring and follow-up observations at a range of wavelengths[17–21] were performed in the direction of this source by the Maser Monitoring Organization (M2O, which is a global cooperative of maser monitoring programmes; https://www.masermonitoring.com). A number of new methanol transitions (about 20 new lines), including the first methanol masers from rotational lines within the first two torsionally excited states ($v_t = 1$ and 2)[17–20] and ^{13}C-substituted isotopic methanol ($^{13}CH_3OH$) transitions[21], have been discovered during this flaring activity. These results indicate that the physical environment during the flaring is peculiar. A factor of two to three increase in the far-infrared flux confirms that the change in the source's physical environment may be due to a burst of accretion onto this HMYSO[19]. The extreme conditions associated with the accretion burst may naturally excite many more maser transitions from methanol and even from other molecules that have not previously been known to show maser emission. In this Letter, we report the discovery of HDO and HNCO maser emission that, combined with the recently reported discovery of an isotopic methanol maser[21], brings the total number of new maser species detected during the current flare to three.

Using the Shanghai 65-m Tianma radio telescope (TMRT), we made the first detection of emission from both HDO $3_{2,1}$–$4_{1,4}$ (20.460 GHz) and HNCO $1_{0,1}$–$0_{0,0}$, $F = 2-1$ (21.981 GHz) transitions in the direction of G358.93-0.03 on 2019 March 17. Higher-resolution follow-up observations were then conducted with the Karl G. Jansky Very Large Array (VLA) on 2019 April 4 to confirm that the detections were masers (see Methods). The spatial distribution and spectra of the HDO and HNCO maser emission derived from the VLA observations are shown in Fig. 1. It can be clearly seen that the spectra of both of the molecular transitions have a narrow velocity range (from −16.5 to −15 km s^{-1}). During the VLA observations, the HDO emission showed a double-peaked profile with maximum flux densities of 3.6 and 1.3 Jy at velocities of −16.2 and −15.4 km s^{-1}, respectively. In comparison, the HNCO emission showed a single peak with a flux density of 2.0 Jy at a velocity of −15.3 km s^{-1}. The HDO maser spots are distributed in two spatial clusters surrounding the HMYSO, which is traced by the dense core of submillimetre continuum emission from MM1 revealed by Atacama Large Millimeter/submillimeter Array (ALMA) observations[20]. Spots showing the HNCO transition are distributed in locations 0.075 arcsec southwest of the HMYSO, corresponding to 520 au at an assumed kinematic distance of 6.7 kpc (estimated using the kinematic Galactic rotation model reported in

[1]Center for Astrophysics, GuangZhou University, Guangzhou, China. [2]Shanghai Astronomical Observatory, Chinese Academy of Sciences, Shanghai, China. [3]Key Laboratory of Radio Astronomy, Chinese Academy of Sciences, Beijing, China. [4]Ural Federal University, Ekaterinburg, Russia. [5]National Astronomical Observatories, Chinese Academy of Science, Beijing, China. [6]SKA Organisation, Jodrell Bank Observatory, Macclesfield, UK. [7]School of Natural Sciences, University of Tasmania, Hobart, Tasmania, Australia. [8]Hartebeesthoek Radio Astronomy Observatory, Krugersdorp, South Africa. [9]The University of Western Ontario, London, Ontario, Canada. [10]Netherlands Institute for Radio Astronomy, Dwingeloo, the Netherlands. [11]The National Radio Astronomy Observatory, Charlottesville, VA, USA. [12]Department of Astronomical Sciences, SOKENDAI (The Graduate University for Advanced Studies), Tokyo, Japan. [13]Mizusawa VLBI Observatory, National Astronomical Observatory of Japan (NAOJ), Tokyo, Japan. [14]Max Planck Institute for Astronomy, Heidelberg, Germany. [15]Max Planck Institute for Radio Astronomy, Bonn, Germany. [16]National Astronomical Research Institute of Thailand (Public Organization), Chiang Mai, Thailand. [17]Thüringer Landessternwarte, Tautenburg, Germany. [18]School of Astronomy and Space Science, Nanjing University, Nanjing, China. ✉e-mail: chenxi@gzhu.edu.cn; andrej.sobolev@urfu.ru

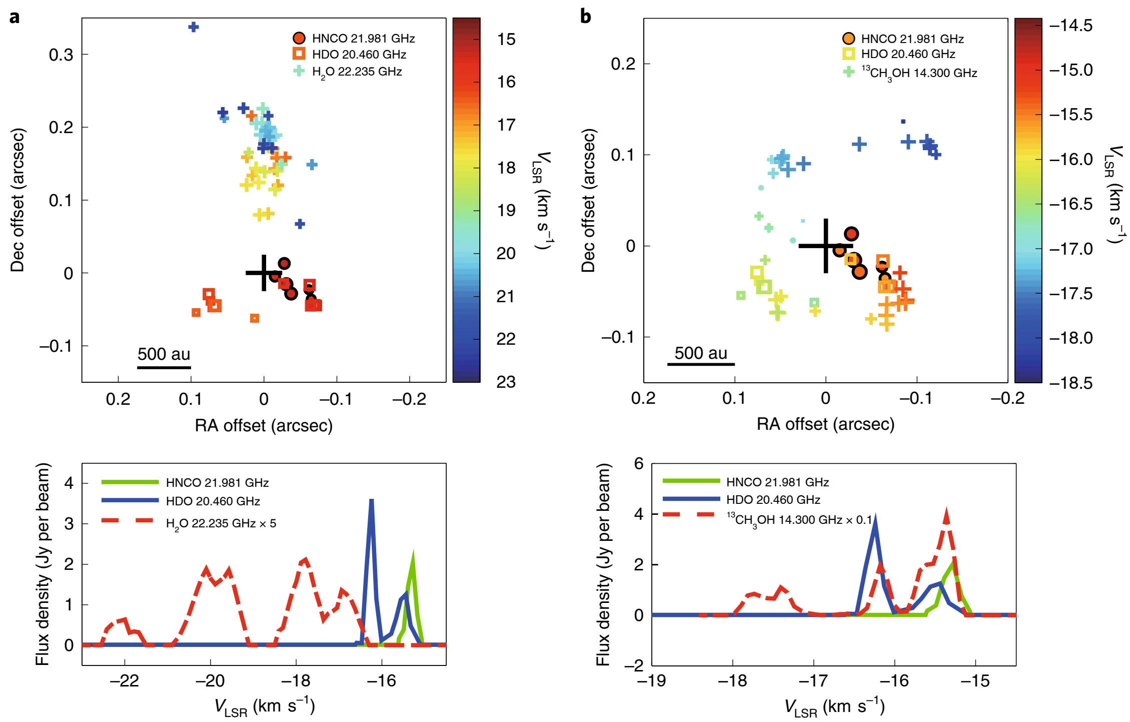

Fig. 1 | Spatial distribution and spectra of multiple molecular maser transitions detected in the direction of G358.93-0.03 with the VLA. a, Spatial distribution (top) and spectra (bottom) for the 20.460 GHz HDO, 21.980 GHz HNCO and 22.235 GHz H_2O maser transitions. **b**, Spatial distribution and spectra for a narrower velocity range to emphasize the spatiokinematic structure of the same HDO and HNCO transitions along with the 14.300 GHz $^{13}CH_3OH$ transition. Each maser spot is represented by a symbol with an area proportional to its flux density (multiplied by 5 for the H_2O maser and 0.1 for the $^{13}CH_3OH$ maser) on a logarithmic scale with a colour indicating its velocity relative to the local standard of rest V_{LSR}. The distribution of the maser emission is relative to the ALMA millimetre continuum source MM1 at right ascension $\alpha = 17$ h 43 min 10.1015 s and declination $\delta = -29°\ 51'\ 45.6936''$ (J2000). The extent of the black plus shows the absolute positional uncertainty (~0.03″) of MM1[20]. The relative positional uncertainty of each maser spot is typically less than 0.01″. The data points shown in this figure are from Supplementary Tables 2–5.

ref. [22] at a systemic source velocity relative to the local standard of rest of $V_{LSR} = -16.5$ km s^{-1}). Part of the HDO maser emission arises to the southwest, from the same location as the HNCO emission, but the brightest HDO maser spots are located about 0.11 arcsec (750 au) southeast of the HMYSO. The brightness temperature range of the detected HDO emission is 3.4×10^2–3.0×10^4 K and 1.2×10^3–1.6×10^4 K for HNCO (see Supplementary Tables 2 and 3). Note that these values are lower limits because these maser spots cannot be distinguished at the angular resolution of the VLA. These lower limits on the brightness temperatures are much higher than the typical kinetic temperatures of 100–400 K for molecular emission from HMYSO hot cores[23], and therefore very probably result from masering.

For comparison, the spatial distribution and spectra of maser emission from the 22.235 GHz H_2O transition detected during the same VLA K-band observations, and the 14.300 GHz 5_1–6_0 A$^+$ $^{13}CH_3OH$ detected in previous VLA Ku-band observations on 2019 March 24 (ref. [21]) are overlaid in Fig. 1. This shows that the velocity ranges of both the HDO and HNCO maser emission only overlap with the redshifted emission from other maser species and that neither of the HDO nor HNCO maser spots are spatially coincident with H_2O masers. In the case of HDO, which shows a completely different spatial distribution and spectral profile to the H_2O maser, this is particularly odd, given that both are isotopologues of the water molecule. The $^{13}CH_3OH$ maser spots, however, show some spatial coincidence with both HNCO and HDO maser spots.

Together, the $^{13}CH_3OH$ masers and HDO and HNCO masers exhibit the morphology of a two-armed spiral feature, as shown in Fig. 1b. One reasonable scheme to explain this structure is that the arms trace accretion flows that proceed onto the central star in spiral trajectories. We used a semi-analytical model to calculate the spatial trajectory and velocity field of the accretion flow. The details of the modelling of the trajectories are described in the Methods and the results of the model are shown in Fig. 2. The observational results can be reproduced with a model that features a central protostar with a mass of $M_* \simeq 12 \pm 3\, M_\odot$ (see Supplementary Table 6).

As seen in Fig. 2b, the optimized model trajectories are consistent with the observed maser spot distributions. The two arms of the accretion flow are modelled independently; each have comparable values for the parameters. In particular, the two flows have very similar inclination angles, suggesting that they originated from the same structure; possibly a disk that later became fragmented. For each arm, the trajectory seems to have a marked turn-over point at radius $r = 0.07$ arcsec (~400 au), where the gas motion turns towards the central star. The two arms (in particular the southern one) also exhibit increasing numbers of maser spots clustered around the turning point. Moreover, both the Long Baseline Array (LBA) observations of 6.7 GHz methanol masers[19] and ALMA observations of (sub)millimetre methanol masers[20] in this source have revealed that those masers are closely clustered at the two turning points. In the model, the turning point is explained by a drastically increased damping force around this radius (see Extended Data Fig. 1). In the scenario of disk fragmentation[1,2], such increased damping would be actually caused by a dense gas structure located at this radius, such as a fragmented clump (see Methods). The inflow would lose much of its angular momentum during the interaction with the clump and

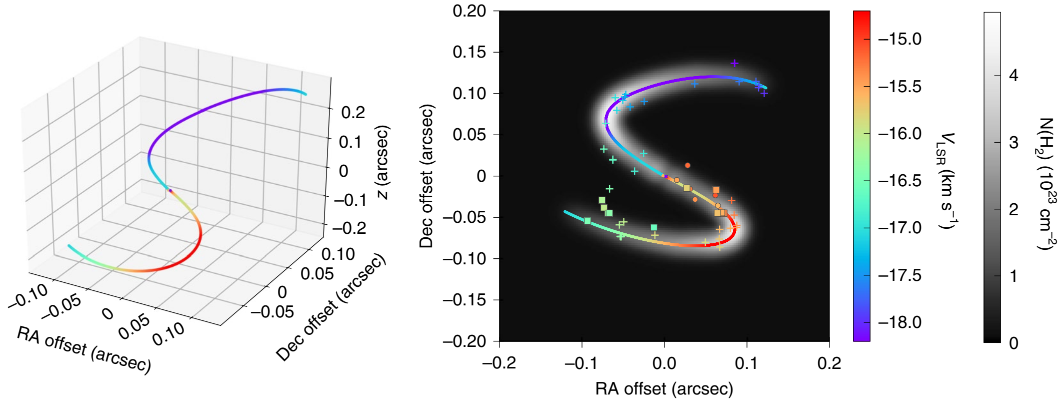

Fig. 2 | Kinematic model results for a two-arm spiral structure traced by HDO, HNCO and $^{13}CH_3OH$ masers. a, The best-fit trajectory in three-dimensional space. The vertical (z) axis is along the line of sight. **b**, The fitted trajectory projected onto the sky-plane. The colour scale applies to **a** and **b**. The background grey-scale image is the total column density distribution of the inflow. The calculation assumes that the inflow has a comparable number density and radius to the individual maser spot; that is, $n_{in}(r_0) = 6\times10^7$ cm^{-3} and radius $\bar{r}_{in} = 100$ au (see Methods) at its starting point (r_0,ϕ_0). The inflow density n_{in} over the trajectory is assumed to be inversely proportional to the total inflow velocity, $v_{in} = [\dot{r}^2 + (r\dot{\phi})^2]^{1/2}$ based on the conservation of the mass flow rate: $v_{in}(r)/v_{in}(r_0) = n_{in}(r_0)/n_{in}(r)$.

then continue inwards towards the star along a more straight path, as shown by the inner part of the trajectory ($r < 0.07$ arcsec).

The theoretical calculations show that the observed HDO and HNCO transitions can produce maser emission under a certain set of physical conditions (see Methods). The results of pumping model calculations for the two transitions are presented in Fig. 3. It can be clearly seen that the maser brightness temperature increases with the increasing prevalence of the dust over the gas temperature. The model results for the HDO maser show consistency with the observed brightness temperatures when the dust temperature exceeds 150 K for both values of the gas temperature. The HNCO maser shows different behaviour—its model brightness temperature is consistent with the observations only when the gas temperature is 100 K but over a wider range of dust temperatures. The calculations suggest that the HNCO maser requires a higher gas temperature for excitation. This is supported by the observation that the HNCO spots are situated closer to the HMYSO (see Fig. 1). The difference between the gas and dust temperatures occurs after the accretion burst, when the increased photon flux ('heat wave' in ref. [19]) reaches the maser region. The temperature of the dust rises much faster than that of the gas. As a result, soon after the burst, the dust is considerably warmer than the gas. The difference between the gas and dust temperatures eventually decreases due to dust radiation and dust–gas collisions. According to our calculations, this leads to the maser emission fading, consistent with observations.

A rapid decline in both the HDO and HNCO maser emission was found in the monitoring observations with the TMRT over the period 2019 April 5–14 (see Methods). Figure 4 shows the variations in peak flux density of the HDO and HNCO spectral features (defined as A and B). For comparison, we also show the variation in the peak flux density of the $^{13}CH_3OH$ maser at velocities close to the HDO and HNCO peaks from the TMRT monitoring during the period 2019 April 2–15 (ref. [21]). It can clearly be seen that these three new species of masers show substantial decay (overall > 50% and up to 90% for some features) in a period of less than half a month. Rapid time-variations of masers are probably related to the changes in the radiation field, and cannot be associated with the process of kinematic material transfer. The changes in the radiation field of G358.93-0.03 have been observed in far-infrared observations that show a considerable increase in luminosity[19]. Such changes may be associated with an accretion burst, possibly caused by disk fragmentation. In this process, the fragmentation of the disk results in the formation of dense clumps that are then rapidly accreted onto the protostar,

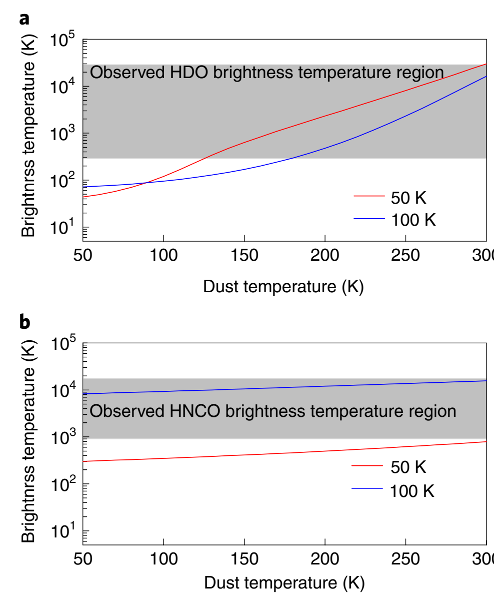

Fig. 3 | The expected brightness temperatures under a radiative–radiative pumping. a,**b**, Expected brightness temperatures for HDO (**a**) and HNCO (**b**) masers. The model calculations were performed for fixed gas temperatures of 50 and 100K, respectively.

causing the accretion luminosity to increase, which in turn causes the emission from common maser lines to brighten, and excites the maser species reported in this work. The unusual maser conditions produced by an accretion burst in G358.93-0.03 are expected to be transient (a timescale of a few months from the M2O project).

At present, the changes in stellar luminosity due to accretion phenomena are studied only on timescales of tens and hundreds of years[24,25] whereas the G358.93-0.03 event has a timescale of only a few months. The influence that the changes in stellar luminosity have on maser brightness is also not well studied and recent research[19,20] (including this paper) only represents the initial stages of the study of the complicated structure of the deeply embedded HMYSO environment. We therefore consider the current research as an important observational input to studies of the relation between burst intensity and the associated maser flaring.

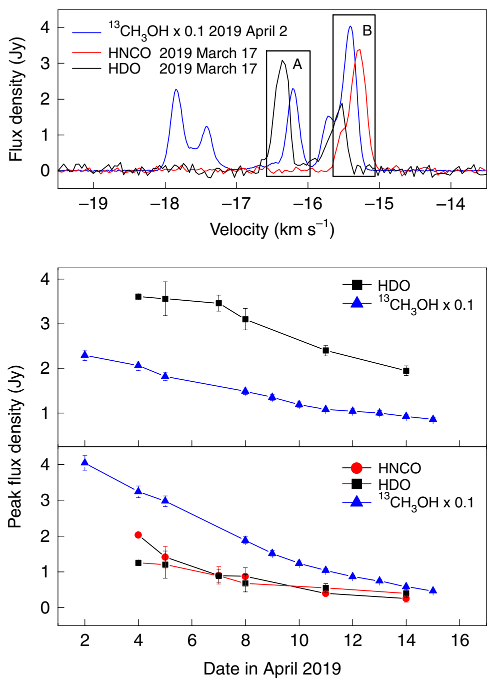

Fig. 4 | The decay in the peak flux density of HDO, HNCO and $^{13}CH_3OH$ maser features obtained from VLA and TMRT observations. Top, example spectra observed with the TMRT on the dates shown. Bottom, variability in the peak flux density of each maser line in the spectral ranges of A and B during the monitoring observation dates. The data for HDO and HNCO on 2019 April 4 were taken with the VLA.

Flaring in the commonly detected 6.7 GHz methanol masers has previously been linked to accretion bursts in NGC6334I-MM1[13,26] and S255NIRS3[14,27]. The accretion burst in G358.93-0.03 shows different properties to the two previously reported cases, including different enhancement in the flux of the 6.7 GHz methanol masers, and a quicker rise and decline of the maser burst[19]. In addition, the two new maser transitions of HDO and HNCO were not detected with TMRT on 2019 May to a root mean square (r.m.s.) noise level of 0.1 Jy in NGC6334I-MM1, although maser emission in the 6.7 GHz CH_3OH line was still showing outburst behaviour at this time, according to monitoring by the M2O project. Together, these differences suggest that G358.93-0.03 may represent a new and unique case for studying high-mass protostellar accretion.

Fragmentation in massive disks due to gravitational instabilities has been predicted to trigger accretion bursts, resulting in observable increases in luminosity[12,13]. At the same time, such instabilities can induce the formation of spiral arms[1–5] that we can detect observationally through morphological changes in the disk[6–10,28,29]. Luminosity bursts and spiral arms, however, had not been linked in the same target. In G358.93-0.03, the distribution of the maser spots from the newly discovered species, determined to high position accuracy (a few tens of au), are consistent with the modelled spiral-arm structures (see Fig. 2). Furthermore, the appearance and disappearance of these new maser species in this source are likely to be associated with a rapidly changing radiation field owing to the accretion burst. This suggests that the new maser species trace both the accretion burst and spiral arms induced by massive disk fragmentation simultaneously, thus providing observational proof linking them to the same disk fragmentation source.

Disk-mediated accretion bursts are often observed in the formation of solar-mass stars, such as FU Orionis objects[30,31]. Our findings further confirm that such a process can occur during the formation of massive stars[14]. Disk-mediated accretion could therefore be considered a common mechanism of star formation from low- to high-mass stars[32–36]. It should be noted that although protostars in both regimes accrete mass from circumstellar disks, high-mass stars have higher disk densities and higher disk-to-star mass ratios, leading to a very different disk evolution due to the (stronger) gravitational instability.

Methods

Observations and data reduction. *TMRT observations.* Observations of the 20.460 GHz HDO and 21.981 GHz HNCO transitions in the direction of G358.93-0.03 were first made with TMRT on 2019 March 17. The molecular line information (see Supplementary Table 1) was retrieved with splatalogue (http://www.cv.nrao.edu/php/splat) and is based on data provided by the Cologne Database for Molecular Spectroscopy (CDMS)[37,38] and the JPL catalogue database[39]. Clear detections of both transitions were made, and their spectra are shown in the top panel of Fig. 4. Subsequent monitoring observations of the two transitions were performed using the TMRT during the period 2019 April 5–April 14 to investigate their variability. The two transitions were observed with the cryogenically cooled K-band receiver and digital backend system, which was configured with two 23.4 MHz spectral windows, each with 4,096 channels (corresponding to a channel spacing of 5.72 kHz or velocity resolution of 0.08 km s^{-1}). The system temperature ranged between 100–150 K during the observations. The beam size was ~45″. Observations were targeted towards the reported 6.7 GHz methanol maser G358.931-0.030 (J2000 position: 17 h 43 min 10.02 s, −29° 51′ 45.8″; ref. [21]). The aperture efficiency of the telescope was ~50%, achieved using active surface correction corresponding to a sensitivity of 1.7 Jy K^{-1}. The uncertainty in the absolute flux density is less than 10%. Observations were conducted in a position-switching mode, with ~30 on–off cycles (and 1 min on and off intervals). The typical r.m.s. noise of the observations was ~0.15 Jy per spectral channel.

For comparison, monitoring data of the 14.300 GHz $^{13}CH_3OH$ maser obtained from TMRT monitoring during the period 2019 April 2–15 are also presented in Fig. 4. The details of these observations are given in ref. [21].

VLA observations. On 2019 April 4 the 20.460 GHz HDO, 21.981 GHz HNCO and 22.235 GHz H_2O maser transitions were observed with the VLA in the B-array configuration. Each of the lines was observed with a 4 MHz band and 512 spectral channels, corresponding to a channel spacing of 0.09 km s^{-1}. The time-dependent antenna gains were calibrated with frequent observations of the quasar J1744-3116 (J2000 position: 17 h 44 min 23.57821 s −31° 16′ 36.2943″). 3C286 was observed to calibrate the bandpass response and flux density. The tracking centre of the observations of G358.93-0.003 was as for the TMRT observations. The visibility data were reduced by the standard VLA calibration pipeline with the common astronomy software applications (CASA 5.3.0) package. The imaging analysis was carried out in ATNF MIRIAD. The resulting synthesized beam size was ~1.35″ × 0.35″. The 3σ detection limit in a single spectral channel was ~50 mJy per beam. We performed a 2D Gaussian brightness distribution fitting using the MIRIAD task IMFIT to estimate the positions and flux densities of the detected maser spots in each channel map. The typical uncertainty in the fitted position of each maser spot was smaller than 0.01 arcseconds (or 70 au at a distance of 6.7 kpc to this source). Supplementary Tables 2–4 list the full parameters measured from the Gaussian fitting of each maser spot for the observed HDO, HNCO and H_2O transitions, respectively.

The spatial distribution and spectra of the 14.300 GHz $^{13}CH_3OH$ transition in the direction of G358.93-0.03 shown in Fig. 1 was achieved from VLA Ku-band observations made on 2019 March 24. The details for the VLA $^{13}CH_3OH$ observations are described in ref. [21]. The full parameters of maser spots for the 14.3 GHz $^{13}CH_3OH$ transition are presented in Supplementary Table 5.

Modelling a two-arm accretion flow traced by the new maser species. The spatial and velocity distributions of the masers suggest that the dense gas is infalling towards the centre in a spiral trajectory. If the infalling gas is originally rotating, there should be a decelerating force from the surrounding medium, including the diffuse gas around the central star and the fragments (or clumps) generated during the disk fragmentation. As shown in hydrodynamical simulations[2], the fragmentation of the massive star-and-disk system would almost inevitably occur during its evolution. The clumps would continue to rotate around the star and interact with the surrounding and infalling gas.

The actual distributions of the fragments and clumps are not well constrained in observations, thus to reasonably estimate the decelerating force to the inflow, we consider only the scenario in which the inflow is interacting with the environmental gas. In this process, the inflow could continuously lose the angular momentum, and inevitably accrete onto the central star in a two-arm trajectory. The two-arm trajectory traced by HDO, HNCO and $^{13}CH_3OH$ masers can be modelled using the Lagrange equation, which describes the motion of a gas element affected by the stellar gravity. The inflow is characterized by a typical radius r_{in} and number density n_{in}; the gas element has a mass of

$$m_{\rm in} = \mu m_{\rm H} n_{\rm in} (4/3)\pi r_{\rm in}^3, \quad (1)$$

where $\mu = 2.33$ is the mean molecular weight. The Lagrangian is

$$L = \frac{m_{\rm in} V^2}{2} + \frac{GM_* m_{\rm in}}{r}, \quad (2)$$

where V is the velocity of the gas element in the inflow and M_* is the stellar mass. V is related to the observed radial velocity as $V_{\rm obs} = (\dot{r}\sin\phi + r\dot{\phi}\cos\phi)\cos i$ and i is the inclination angle between the rotating structure plane and the line of sight. The spiral trajectory plane would correspond to the original disk around the star. The equation is

$$\frac{\mathrm{d}}{\mathrm{d}t}\frac{\partial L}{\partial \dot{q}_j} - \frac{\partial L}{\partial q_j} + \frac{\partial P_r}{\partial \dot{q}_j} = 0. \quad (3)$$

In the equation, P_r acts as a perturbation term, representing the kinetic energy loss rate during the deceleration caused by the interaction with surrounding medium, which can be written

$$P_r = \frac{1}{2}\gamma m_{\rm in} V^2, \quad (4)$$

Its derivative to the velocity is the expression F_r, that is

$$F_r = \frac{\mathrm{d}P_r}{\mathrm{d}V} = \gamma m_{\rm in} V, \quad (5)$$

where γ is the damping factor, which characterizes the resistance (or damping) to the gas element in the inflow. We expect it to be proportional to the environmental gas density $n(r)$ if the decelerating force is dominated by the hydrodynamical interaction. Here we adopt a quasi-power-law density profile of

$$n(r) = \frac{n_0}{1 + (r/r_0)^\alpha}, \quad (6)$$

where the expression of the denominator is adopted to prevent the central singularity. It would approximate the power-law form towards large r. The $\gamma(r)$ profile accordingly has a similar form of

$$\gamma(r) = \frac{\gamma_0}{1 + (r/r_0)^\alpha}. \quad (7)$$

We expect r_0 to be comparable to the radius at the turning point, where the deceleration becomes important so that the gas flow is being rapidly redirected to the centre. Although the conversion factor between $\gamma(r)$ and $n(r)$ is largely unknown, we have a qualitative expectation that $\gamma(r)$ would be relatively small when $n(r) \ll n_{\rm in}$, and would become important if $n(r)$ and $n_{\rm in}$ are comparable. The inflow could have a comparable density to the maser spots (see the next section), namely $n_{\rm in} \simeq n_{\rm maser} = 5.6\times10^7\,{\rm cm^{-3}}$.

If letting $q_j = r$ and $q_j = \phi$, equation (3) transforms into the following system of equations, where G is the gravitational constant

$$\ddot{r} - r\dot{\phi}^2 + \frac{GM_*}{r^2} + \frac{\gamma_0 \dot{r}}{1 + (r/r_0)^\alpha} = 0, \quad (8)$$

$$\ddot{\phi} + \frac{2\dot{r}\dot{\phi}}{r} + \frac{\gamma_0 \dot{\phi}}{1 + (r/r_0)^\alpha} = 0, \quad (9)$$

One can numerically rebuild the trajectory by running equations (8) and (9) with small steps of r and ϕ. The parameter set that results in the best fit to the observed maser spots has been achieved by manually adjusting the input parameters that determine various aspects of the trajectory. We inspected a large range of parameter space. The quality of model fitting is evaluated from the deviation between the model trajectory and the observed maser points in the position and velocity space. When the trajectory becomes reasonably coincident with the observed masers, we let each parameter vary by 50% around the observed value to look for the 'optimized' parameters that lead to the smallest deviation. It guarantees that the model trajectory is the best fit in this local parameter space, namely from 0.5 to 1.5× the optimized values. The best-fit parameters are presented in Supplementary Table 5. We note that the parameters $r_{\rm in}$, $n_{\rm in}$ and n_0 are not determined in our current model; $m_{\rm in}$ also cannot be individually determined because it depends on the parameters $r_{\rm in}$ and $n_{\rm in}$ from equation (1).

Although the model depends on multiple input parameters that are not constrained to an high accuracy, it exhibits three clear features. First, the model consistently shows the existence of a central high-mass star (~12 $M_\odot$). Second, as divided by the turning point, the outer part ($r > r_0$) and inner part ($r < r_0$) of the spiral inflow have different kinematical properties. The outer part mainly features rotation, whereas the inner part is mostly dominated by the infall motion, and the velocity field is noticeably consistent with the observed maser spots. The velocity field of the inner part cannot be explained by pure rotation unless the rotational axis is considerably different from the outer part. Combining the model and observed masers demonstrates that the inflow proceeds around the central star.

The third and most important feature is that the turning point is dynamically determined by the $\gamma(r)$, and thus the $n(r)$, profile. To generate the turning point, the $n(r)$ profile has to drastically increase around r_0 (see Extended Data Fig. 1). This is unusual for a spherical dense core. However, it suggests another possibility: that the inflow may have encountered a particular high-density structure around r_0. Such structures could exist in the scenario of disk fragmentation. The simulations show that the fragments would usually be generated in various physical conditions and assembled into clumps and finger-like structures[2]. These structures would continue to interact with the surrounding gas, thereby sustaining the stellar accretion after the major disk structure is fragmented. This is in noticeable consistency with the inflow velocity field, as well as the clustered maser spots at the southern turning point. Moreover, we see that the peak damping factor of $\gamma_0 = 10^{-11}\,{\rm s^{-1}}$ corresponds to ~1.5 orbits (~620 au) at the location of the turning point (410 au) around a 12 $M_\odot$ star, indicating that the decelerated accretion flow or fragment can migrate to the high-mass protostar in such a timescale. In agreement with these analytical considerations, the simulation also suggests a typical migration timescale of the forming fragments of 1–2 orbits[1,2].

The gravity of the clump may be involved in the interaction with the infall. To be specific, a fragment or accretion flow (named A) is on an unperturbed orbit until it approaches a fragment (named B) at the turning point. B exerts a gravitational torque on A and decelerates it along its orbital motion. As a consequence, the stellar gravity acting on A is no longer in equilibrium with the centrifugal force, and A quickly migrates towards the protostar. Accretion flow (or fragment) interactions with fragments seem to also agree with the damping curve, which resembles a sudden impact.

Pumping model for the HNCO and HDO masers. The main goal of the pumping model here is to explain the following observational facts:

(1) There is maser emission in both HDO $3_{2,1}$–$4_{1,4}$ (20.460 GHz) and HNCO $1_{0,1}$–$0_{0,0}$, $F = 2-1$ (21.981 GHz) transitions.
(2) HNCO maser emission comes from locations southwest of the HMYSO with the angular distances up to 0.075 arcsec from the HMYSO. At a distance of 6.7 kpc, this corresponds to 520 au. HDO maser emission sometimes comes from the same locations as the HNCO emission, but the brightest spots have different locations at about 0.11 arcsec (750 au) southeast of the HMYSO.
(3) HNCO and HDO maser spots do not coincide in position with the spots of H_2O maser, but they are close to $^{13}CH_3OH$ maser spots.
(4) HDO and $^{13}CH_3OH$ spots form clusters with a characteristic size at about 100 au along the arms, but HNCO maser spots probably form one cluster with a larger size positioned from 100 au to 400 au southwest of the HMYSO.

Observational fact (3) tells us that no HNCO and HDO maser spots coincide in position with that of the H_2O maser, which has a collisional–radiative pumping mechanism[40]. At the same time, some of the HNCO and HDO maser spots coincide in position with $^{13}CH_3OH$ maser, which has a radiative–radiative pumping mechanism[41]. Our HNCO and HDO masers are therefore likely to also have a radiative–radiative pumping mechanism that can be reproduced by models similar to those presented in refs. [42,43]. The model is implemented in a custom code (see https://github.com/ParfenovS/LVG_LRT) and utilizes spectroscopic data for HDO and HNCO molecules from the LAMDA database[44]. The basic model parameters are specific column density of the masering molecule, internal gas density and temperature, external dust parameters and the background emission. The external dust parameters include the dust temperature, dilution factor, $W_{\rm d}$, optical depth and the grain opacity spectral index. We constrain the model parameters with the following considerations.

CH_3OH masers are quenched at densities $\sim1.0\times10^8\,{\rm cm^{-3}}$ and achieve their maximum brightness with densities $\sim1.0\times10^{7.75}\,{\rm cm^{-3}}$ ($=5.6\times10^7\,{\rm cm^{-3}}$; see ref. [43]). $^{13}CH_3OH$ masers have a similar dependence on the density. Some of HDO and HNCO maser spots coincide with $^{13}CH_3OH$ ones in position (observational fact (3)). These masers are thus produced at similar densities. We therefore assumed that the hydrogen number density in the maser clump is $5.6\times10^7\,{\rm cm^{-3}}$. We assume that the size of the maser clump is approximately equal to the size of the maser cluster: 100 a.u. Maser spectral line features have a full-width at half-maximum of ~0.1 km s^{-1} (the same as the spectral resolution of the VLA observations). We therefore used this value for the estimates of specific column density. The resulting H_2 specific column density of the model maser clump is $N_{\rm H_2}/\Delta V \approx 8.4\times10^{18}\,{\rm cm^3\,s^{-1}}$. According to fig. 12 in ref. [45], the relative [HNCO/H_2] abundance ratio in the vicinity of a HMYSO can reach values of $\sim3\times10^{-7}$. Thus the HNCO specific column density of the clump can be $N_{\rm HNCO}/\Delta V = 3\times10^{-7} N_{\rm H_2}/\Delta V = 2.5\times10^{12}\,{\rm cm^{-3}\,s^{-1}}$. According to ref. [46], [H_2O/H_2] in the massive star formation region Orion KL can reach the $\sim6.5\times10^{-4}$. The value of [HDO/H_2O] these authors determine is 0.003. The relevant value of [HDO/H_2] is 2×10^{-6}. So, assuming that the HDO abundance in G358.93-0.03 is similar to that in Orion KL, the HDO specific column density of the clump could be about $N_{\rm HDO}/\Delta V = 2\times10^{-6} N_{\rm H_2}/\Delta V = 1.7\times10^{13}\,{\rm cm^{-3}\,s^{-1}}$. We used a grain opacity spectral index of 1.7 (ref. [20]) and assumed that the frequency at which the dust emission becomes optically thick is 337.08 GHz (as suggested by ref. [20]). The background emission was the cosmic microwave background, with a temperature of 2.7 K.

Other model parameters are not constrained and can be used as free parameters in the pumping model. We performed the calculations of the model grid by varying W_d in the range of [0,1], dust and gas temperatures in the range of [50 K,300 K]. Our calculations show that brightness temperatures similar to the observed ones for both HDO and HNCO masers can be achieved in the models with $W_d = 1$ and with dust temperatures exceeding the gas temperature. The brightness temperatures calculated for the HNCO maser with $N_{HNCO}/\Delta V = 2.5\times10^{12}\,cm^{-3}\,s^{-1}$ are relatively low in comparison with the limits derived from observations and do not exceed 2,100 K. The highest observed brightness temperatures can be modelled with $N_{HNCO}/\Delta V = 3.5\times10^{12}\,cm^{-3}\,s^{-1}$. This specific column density can be achieved by increasing the HNCO abundance to 4.5×10^{-7}, which is consistent with estimates given by ref. [45] within the bounds of uncertainties, and/or by increasing the maser clump size up to 140 au, which is consistent with the observed HNCO maser cluster size.

We also performed the calculations for the H_2O maser for physical conditions similar to those used for the HDO and HNCO calculations with the spectroscopic data from LAMDA and a specific column density of $N_{H_2O}/\Delta V = 6.5\times10^{-4} N_{H_2}/\Delta V = 5.5\times10^{15}\,cm^{-3}\,s^{-1}$. The calculations show that the H_2O masers are not excited in the physical conditions in which the HDO and HNCO masers are excited (observational fact (3)).

Data availability

The data from both TMRT and VLA that support the plots within this paper and other findings of this study are available from X.C. on reasonable request. Source data are provided with this paper.

Code availability

The code for the pumping model of HDO and HNCO masers is available at https://github.com/ParfenovS/LVG_LRT

Received: 19 March 2020; Accepted: 4 June 2020;
[redacted]

References

1. Meyer, D. M.-A., Vorobyov, E. I., Kuiper, R. & Kely, W. On the existence of accretion-driven bursts in massive star formation. *Mon. Not. R. Astron. Soc.* **464**, L90–L94 (2017).
2. Meyer, D. M.-A., Kuiper, R., Kley, W., Johnston, K. G. & Vorobyov, E. Forming spectroscopic massive protobinaries by disc fragmentation. *Mon. Not. R. Astron. Soc.* **473**, 3615–3637 (2018).
3. Meyer, D. M.-A. et al. On the ALMA observability of nascent massive multiple systems formed by gravitational instability. *Mon. Not. R. Astron. Soc.* **487**, 4473–4491 (2019).
4. Ahmadi, A., Kuiper, R. & Beuther, H. Disc kinematics and stability in high-mass star formation: linking simulations and observations. *Astron. Astrophys.* **632**, A50 (2019).
5. Jankovic, M. R. et al. Observing substructure in circumstellar discs around massive young stellar objects. *Mon. Not. R. Astron. Soc.* **482**, 4673–4686 (2019).
6. Johnston, K. G. et al. Spiral arms and instability within the AFGL 4176 mm1 disc. *Astron. Astrophys.* **634**, L11 (2020).
7. Maud, L. T. et al. The ALMA view of W33A: a spiral filament feeding the candidate disc in MM1-Main. *Mon. Not. R. Astron. Soc.* **467**, L120–L124 (2017).
8. Maud, L. T. et al. Substructures in the Keplerian disc around the O-type (proto-)star G17.64+0.16. *Astron. Astrophys.* **627**, L6 (2019).
9. Ilee, J. D. et al. G11.92-0.61 MM 1: a fragmented Keplerian disk surrounding a proto-O Star. *Astrophys. J. Lett.* **869**, L24 (2018).
10. Motogi, K. et al. The first birds-eye view of a gravitationally unstable accretion disk in high-mass star formation. *Astrophys. J. Lett.* **877**, L25 (2019).
11. Laughlin, G. & Bodenheimer, P. Nonaxisymmetric evolution in protostellar disks. *Astrophys. J.* **436**, 335–354 (1994).
12. Meyer, D. M.-A. et al. Burst occurrence in young massive stellar objects. *Mon. Not. R. Astron. Soc.* **482**, 5459–5476 (2019).
13. Hunter, T. R. et al. An extraordinary outburst in the massive protostellar system NGC6334I-MM1: quadrupling of the millimeter continuum. *Astrophys. J. Lett.* **837**, L29 (2017).
14. Garatti, A. C. O. et al. Disk-mediated accretion burst in a high-mass young stellar object. *Nat. Phys.* **13**, 276–279 (2017).
15. Sugiyama, K., Saito, Y., Yonekura, Y. & Momose, M. Bursting activity of the 6.668-GHz CH_3 OH maser detected in G 358.93-00.03 using the Hitachi 32-m. *Astron. Telegr.* **12446** (2019).
16. Caswell, J. L. et al. The 6-GHz methanol multibeam maser catalogue: I. Galactic Centre region, longitudes 345° to 6°. *Mon. Not. R. Astron. Soc.* **404**, 1029–1060 (2010).
17. Breen, S. L. et al. Discovery of six new class II methanol maser transitions, including the unambiguous detection of three torsionally excited lines toward G358.931-0.030. *Astrophys. J. Lett.* **876**, L25 (2019).
18. MacLeod, G. C. et al. Detection of new methanol maser transitions associated with G358.93-0.03. *Mon. Not. R. Astron. Soc.* **489**, 3981–3989 (2019).
19. Burns, R. A. et al. A heatwave of accretion energy traced by masers in the G358-MM1 high-mass protostar. *Nat. Astron.* **4**, 506–510 (2020).
20. Brogan, C. L. et al. Sub-arcsecond (sub)millimeter imaging of the massive protocluster G358.93-0.03: discovery of 14 new methanol maser transitions associated with a hot core. *Astrophys. J. Lett.* **881**, L39 (2019).
21. Chen, X. et al. $^{13}CH_3OH$ masers associated with an accretion burst in high-mass young stellar object. *Astrophys. J. Lett.* **890**, 22 (2020).
22. Reid, M. J., Dame, T. M., Menten, K. M. & Brunthaler, A. A parallax-based distance estimator for spiral arm sources. *Astrophys. J.* **823**, 77 (2016).
23. Hernández-Hernández, V., Zapata, L., Kurtz, S. & Garay, G. SMA millimeter observations of hot molecular cores. *Astrophys. J.* **786**, 38 (2014).
24. Meyer, D. M., Haemmerlé, L. & Vorobyov, E. I. On the episodic excursions of massive protostars in the Hertzsprung Russell diagram. *Mon. Not. R. Astron. Soc.* **484**, 2482–2498 (2019).
25. Hosokawa, T., Yorke, H. W. & Omukai, K. Evolution of massive protostars via disk accretion. *Astrophys. J.* **721**, 478 (2010).
26. Hunter, T. R. et al. The extraordinary outburst in the massive protostellar system NGC 6334I-MM1: emergence of strong 6.7 GHz methanol masers. *Astrophys. J.* **854**, 170 (2018).
27. Moscadelli, L. et al. Extended CH_3 OH maser flare excited by a bursting massive YSO. *Astron. Astrophys.* **600**, L8 (2017).
28. Izquierdo, A. F. et al. Radiative transfer modelling of W33A MM1: 3D structure and dynamics of a complex massive star-forming region. *Mon. Not. R. Astron. Soc.* **478**, 2505–2525 (2018).
29. Liu, H. B. et al. ALMA resolves the spiraling accretion flow in the luminous OB cluster-forming region G33.92.0.11. *Astrophys. J.* **804**, 37 (2015).
30. Audard, M. et al. in *Protostars and Planets VI* (eds Beuther, H. et al.) 387–410 (Univ. Arizona Press, 2014).
31. Reipurth, B. & Aspin, C. in *Evolution of Cosmic Objects through their Physical Activity: Victor Ambartsumian Centennial Volume* (eds Harutyunyan, H. et al.) 19–38 (Gitutyun, 2010).
32. Nakano, T. Conditions for the formation of massive stars through nonspherical accretion. *Astrophys. J.* **345**, 464–471 (1989).
33. Jijina, J. & Adams, F. C. Infall collapse solutions in the inner limit: radiation pressure and its effects on star formation. *Astrophys. J.* **462**, 874–887 (1996).
34. Krumholz, M. R., Klein, R. I., McKee, C. F., Offner, S. S. R. & Cunningham, A. J. The formation of massive star systems by accretion. *Science* **323**, 754–757 (2009).
35. Kuiper, R., Klahr, H., Beuther, H. & Henning, T. Circumventing the radiation pressure barrier in the formation of massive stars via disk accretion. *Astrophys. J.* **722**, 1556–1576 (2010).
36. Kuiper, R., Klahr, H., Beuther, H. & Henning, T. Three-dimensional simulation of massive star formation in the disk accretion scenario. *Astrophys. J.* **732**, 20 (2011).
37. Müller, H. S. P., Thorwirth, S., Roth, D. A. & Winnewisser, G. The Cologne Database for Molecular Spectroscopy, CDMS. *Astron. Astrophys.* **370**, L49–L52 (2001).
38. Müller, H. S. P., Schlöder, F., Stutzki, J. & Winnewisser, G. The Cologne Database for Molecular Spectroscopy, CDMS: a useful tool for astronomers and spectroscopists. *J. Mol. Struct.* **742**, 215–227 (2005).
39. Pickett, H. M. et al. Submillimeter, millimeter, and microwave spectral line catalog. *J. Quant. Spectrosc. Radiat. Transfer* **60**, 883–890 (1998).
40. Gray, M *Maser Sources in Astrophysics.* (Cambridge Univ. Press, 2012).
41. Johns, K. P., Cragg, D. M., Godfrey, P. D. & Sobolev, A. M. Class II maser candidates in substituted methanol: CH_3 OD, ^{13} CH_3 OH, $CH_3{}^{18}$ OH and CH_3 SH. *Mon. Not. R. Astron. Soc.* **300**, 999–1005 (1998).
42. Sobolev, A. M. & Deguchi, S. Pump cycles and population flow networks in astrophysical masers: an application to class II methanol masers with different saturation degrees. *Astrophys. J.* **433**, 719–724 (1994).
43. Cragg, D. M., Sobolev, A. M. & Godfrey, P. D. Models of class II methanol masers based on improved molecular data. *Mon. Not. R. Astron. Soc.* **360**, 533–545 (2005).
44. Schöier, F. L., van der Tak, F. F. S., van Dishoeck, E. F. & Black, J. H. An atomic and molecular database for analysis of submillimetre line observations. *Astron. Astrophys.* **432**, 369 (2005).
45. Gieser, C. et al. Chemical complexity in high-mass star formation: an observational and modeling case study of the AFGL 2591 VLA 3 hot core. *Astron. Astrophys.* **631**, A142 (2019).
46. Neill, J. L. et al. The abundance of H_2O and HDO in Orion Kl from Herschel/HIFI. *Astrophys. J.* **770**, 142 (2013).

Acknowledgements

We thank TMRT and VLA staff for their assistance in obtaining the data presented in this paper. The National Radio Astronomy Observatory is a facility of the National Science

Foundation operated under agreement by the Associated Universities, Inc. X.C. was supported by the National Natural Science Foundation of China (grant numbers 11590781, 11873002, 12011530065 and 11590780), Guangdong Province Universities and Colleges Pearl River Scholar Funded Scheme (2019), Astronomy Science and Technology Research Laboratory of Department of Education of Guangdong Province, and Key Laboratory for Astronomical Observation and Technology of Guangzhou. A.M.S. and S.P. were supported by the Russian Science Foundation (grant number 18-12-00193). S.P.E. acknowledges the support of an ARC Discovery Project (project number DP180101061).

Author contributions
X.C. and A.M.S. wrote the initial manuscript, obtained and reduced the data, and led the initial observing proposals. Z.-Y.R. carried out the kinematic model analysis for the maser spots. S.P. performed the pumping model calculations for the masers. S.L.B., S.P.E. Z.-Q.S. and B.L. were involved in the initial observing proposal of the VLA and TMRT and helped to improve the manuscript. G.C.M., W.B., C.B., T.H., T.R.H., H.L., K.M., K.S., B.S., Y.G. and X.Z. are members of the M2O group and helped improve to the text.

Competing interests
The authors declare no competing interests.

Additional information
Extended data is available for this paper at https://doi.org/10.1038/s41550-020-1144-x.

Supplementary information is available for this paper at https://doi.org/10.1038/s41550-020-1144-x.

Correspondence and requests for materials should be addressed to X.C. or A.M.S.

Reprints and permissions information is available at www.nature.com/reprints.

Publisher's note Springer Nature remains neutral with regard to jurisdictional claims in published maps and institutional affiliations.

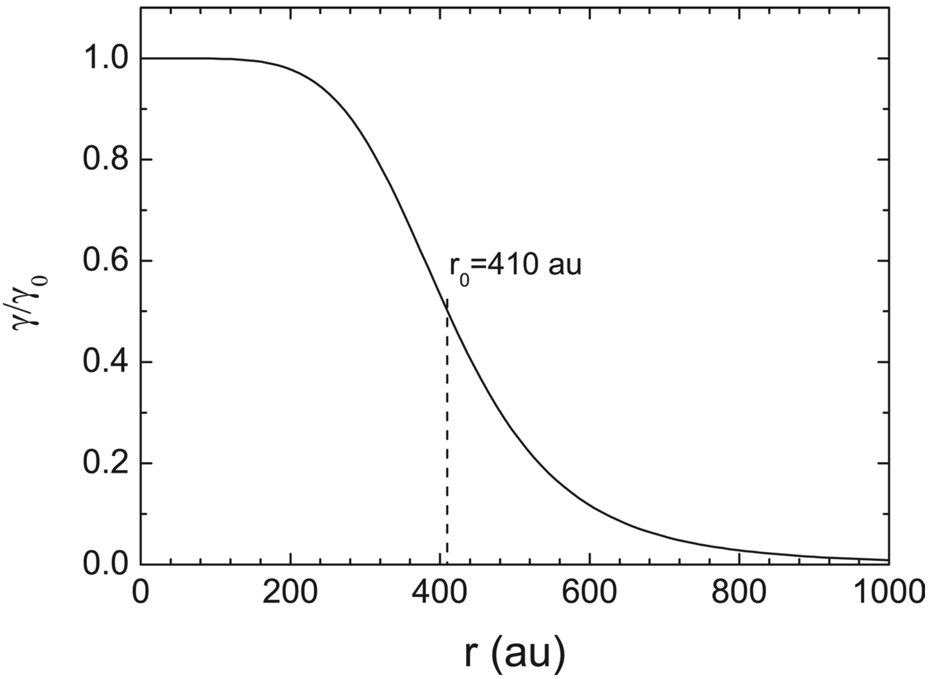

Extended Data Fig. 1 | The damping factor γ/γ_0 as a function of distance from center protostar. The vertical dashed line denotes the position of turning point (r_0 =410 au).